Toy model of turbulent shear flow using vortons

Wandrille Ruffenach
ENS de Lyon, CNRS, LPENSL, UMR5672, 69342, Lyon Cedex 07, France
and Université Paris-Saclay, CEA, CNRS, SPEC, 91191, Gif-sur-Yvette, France

Lucas Fery
Laboratoire des Sciences du Climat et de l'Environnement, CEA Saclay l'Orme des Merisiers, UMR 8212 CEA-CNRS-UVSQ, Université Paris-Saclay and IPSL, Paris, France,
and Université Paris-Saclay, CEA, CNRS, SPEC, 91191, Gif-sur-Yvette, France

Bérengère Dubrulle*
Université Paris-Saclay, CEA, CNRS, SPEC, 91191, Gif-sur-Yvette, France

(Received 20 December 2024; accepted 10 April 2025; published 1 May 2025)

We introduce a toy model for shear flows, exploiting the spatial intermittency and the scale separation between large-scale flows and small-scale structures. The model is highly sparse, focusing exclusively on the most intense structures, which are represented by vortons—dynamically regularized quasisingularities that experience rapid distortion from the large-scale shear. The vortons, in turn, influence the large-scale flow through the subgrid stress tensor. Despite its simplicity, the model displays an interesting transition between two distinct regimes: (i) a laminar regime, where dissipation is entirely attributed to the large-scale flow and the vortons dynamics is essentially diffusive, and (ii) a turbulent regime, in which most of the dissipation arises from the vortons. These regimes correspond to different scalings of dissipation and the Grashof number as functions of the Reynolds number, with power-law relationships that resemble those observed in classical turbulence.

DOI: 10.1103/PhysRevFluids.10.054601

I. INTRODUCTION

Near-wall turbulence arises in many industrial or geophysical flows. With respect to other types of turbulence, it is peculiar in several aspects: (i) it is anisotropic; (ii) it is very intermittent, both in space and time, and both at the turbulent transition or later; (iii) it is nonlocal, and piloted by interactions between the large-scale shear and the small-scale turbulent structures. These three aspects make its modeling challenging, as traditional large eddy simulations have difficulties to resolve the near-wall structures, and traditional RANS model do not capture the spatial or temporal intermittency.

These observations motivated the introduction of nonlocal models, based on the two-way coupling between large-scale shear and small-scale vorticity wave packets [1,2]. On the one hand, the action of large scales onto small scales is described by rapid distorsion theory (RDT), where small scales are advected and sheared by the mean shear. On the other hand, the small scales act on the large scales via the Reynolds stress. The small scales correspond to debris from coherent vortices generated in the viscous sublayer that penetrate in the overlap region and provide a continuous forcing, allowing us to reach a statistically steady state. In such a setting, analytical computations

*Contact author: berengere.dubrulle@cea.fr

are possible both in 2D and 3D and lead to the celebrated log-law of the wall [1,2] or to the complete description of equilibrium velocity profiles in plane parallel flows [3]. These computations are limited to the regime where turbulence is weak, so nonlinear interactions between the small-scale vorticity packets is neglected. This somehow limits the interest of the model to understand the physics of shear flows.

Including nonlinear interactions is, however, challenging, as it may require the integration of the partial differential Navier-Stokes equations in 3D, making the corresponding model too computationally involved to be of any practical use. In this paper, we show that it is possible to avoid the appeal to partial differential equations by using Novikov's vorton approximation, in which the small-scale vorticity is described by pointlike singularities, named vortons, that interact nonlinearly following Biot-Savart law and the discretized inviscid Euler equation. In such a setting, the partial differential equations can be replaced by a set of coupled ordinary differential equations that describe the interactions between the N vortons. This provides the third mechanism that is missing in the RDT theory of Refs. [1–3], opening the way to interesting applications. Specifically, we show in the present paper that using only 27 vortons, we are able to reproduce several features of near-wall turbulence, such as the laminar to turbulent transition or the log-normal statistics of the energy dissipations. The resulting toy model that is both sparse and computationally cheap may then be seen as a promising tool to explore nonlinear interactions in shear flows.

II. NOVIKOV MODEL

A. Equations

Our model builds from Novikov's model, which belongs to a more general class of vortex particle methods [4,5]. In those methods, the vorticity field is discretized into localized vortices of given circulation that are advected by the flow. In two dimensions of space, vorticity is a Lagrangian invariant of the Euler equation and discretizing the vorticity field naturally leads to the famous Onsager vortex gas model, predicting the condensation of energy at large scales [6]. In three dimensions, however, the vorticity stretching term in the Euler equation (1) changes the picture:

$$\frac{\mathrm{D}\boldsymbol{\omega}}{\mathrm{D}t} = (\boldsymbol{\omega}\cdot\nabla)\boldsymbol{u}, \tag{1}$$

$$= (\boldsymbol{\omega}\cdot\nabla^{\mathrm{T}})\boldsymbol{u}. \tag{2}$$

To find approximate solutions of the Euler equations (1) and following the ideas of the two-dimensional point vortices, Novikov [7] introduced the *vortons* model. These Lagrangian vortex particles, located at position $\boldsymbol{x}_\alpha$ and with circulation (vorticity times a volume) $\boldsymbol{\gamma}_\alpha$ generate a vorticity field of the form

$$\boldsymbol{\omega}(\boldsymbol{x},t) = \sum_\beta \boldsymbol{\gamma}_\beta(t)\delta(\boldsymbol{x}-\boldsymbol{x}_\beta(t)). \tag{3}$$

The velocity field is recovered using the Biot-Savart law,

$$\boldsymbol{u}(\boldsymbol{x},t) = -\frac{1}{4\pi}\sum_\beta \frac{\boldsymbol{x}-\boldsymbol{x}_\beta}{\|\boldsymbol{x}-\boldsymbol{x}_\beta\|^3}\times\gamma_\beta, \tag{4}$$

and is by construction divergence-free. The fields (3) and (4) associated with Euler equation (1) in a Lagrangian framework yield the time evolution for the variables $\boldsymbol{x}_\alpha$ and $\boldsymbol{\gamma}_\alpha$,

$$\begin{aligned}\dot{\boldsymbol{x}}_\alpha(t) &= \boldsymbol{u}(\boldsymbol{x}_\alpha,t)\\ \dot{\boldsymbol{\gamma}}_\alpha(t) &= [\nabla\boldsymbol{u}(\boldsymbol{x}_\alpha,t)]\boldsymbol{\gamma}_\alpha,\end{aligned} \tag{5}$$

where the velocity field $\boldsymbol{u}(\boldsymbol{x}_\alpha, t)$ and its gradient $\nabla \boldsymbol{u}(\boldsymbol{x}_\alpha, t)$ are evaluated with (4) but without the $\alpha = \beta$ term in the sum to avoid the unphysical behavior caused by the singularity of the model at the origin.

B. Drawbacks of Novikov model and its modifications

The Novikov model presents several flaws:

(i) The vorticity field (3) is not divergence-free, in general, and, if so, will not remain under time evolution. This issue can be tackled by considering other discretizations of the vorticity field, such as Ref. [8].

(ii) The vorton model cannot generate a statistically steady state. Indeed, for a system of two vortons obeying (5), Novikov [7] showed that $\|\boldsymbol{\gamma}_\alpha(t)\|$ diverges exponentially with time for a given set of initial conditions.

(iii) The fields generated by $\boldsymbol{x}_\alpha$, $\boldsymbol{\gamma}_\alpha$ with dynamical system (5) are not a solution (in the weak sense) of Euler equations (1) [9].

This last problem precludes the use of the Novikov model to simulate Euler equations. To address this drawback, a modification of the model was proposed, based on a remark by Ref. [10]. Due to the nonsolenoidal character of the vorticity, solutions of the Novikov model are such that $\boldsymbol{\omega} \neq \nabla \times u$. As a consequence, the Euler equation (1) and its transposed version (2) are not equivalent. It turns out that if we now keep $\boldsymbol{\omega}$ and $\boldsymbol{u}$ given by (3) and (4), using the transposed scheme, the system

$$\begin{aligned} \dot{\boldsymbol{x}}_\alpha(t) &= \boldsymbol{u}(\boldsymbol{x}_\alpha, t) \\ \dot{\boldsymbol{\gamma}}_\alpha(t) &= [\nabla \boldsymbol{u}(\boldsymbol{x}_\alpha, t)]^{\mathrm{T}} \boldsymbol{\gamma}_\alpha \end{aligned} \tag{6}$$

yields a weak solution [11] of the Euler equations (2) and conserves key physical quantities such as the total vorticity [10] or helicity.

However, this modification itself still presents two drawbacks:

(i) The transposed vorton model cannot generate a statistically steady state. Indeed, like in the original vorton model with $N \geqslant 2$ vortons, a random initial condition, the quantity

$$\Gamma(t) = \sum_{\alpha=1}^{N} \|\boldsymbol{\gamma}_\alpha(t)\|^2 \tag{7}$$

would most surely be divergent in time, making any turbulentlike stationary regime unreachable.

(ii) In its original philosophy, this model is just an alternative way to solve the Euler equations. The equivalence between this method and the Euler equation is then guaranteed only in the limit where one can add indefinitely many vortons in the system as time passes by and vortex filaments are getting stretched, resulting in vortons moving apart far from each other, breaking the continuous line approximation.

These difficulties combined with the flaws mentioned earlier restricted the use of this kind of model to simple situations such as vortex line interactions or vortex rings leap-frogging, for instance [7].

III. A NEW MODEL FOR SHEAR FLOWS

A. General picture

The model we consider is based on several ideas that are meant to correct the main drawbacks identified earlier.

Idea 1: Sparsity. Instead of considering vortons as elementary blocks used to decompose the whole vorticity field—which implies the consideration of many vortons—we instead consider that vortons model the few extreme events of vorticity arising in the flow, extremes that will be the main

players to pilot the full flow dynamics. In that approximation, we can keep only a few vortons as time passes by, as extreme events are, by definition, isolated and rare events.

Idea 2: Regularization. To avoid runaway of the vorton energy and allow for stationary states, we introduce an effective size for the vortex cores. This is done by mollifying the vorticity field

$$\begin{aligned}\omega_\eta(\boldsymbol{x},t) &= (\zeta_\eta * \omega)(\boldsymbol{x},t)\\ &= \sum_\beta \zeta_\eta(\boldsymbol{x}-\boldsymbol{x}_\beta(t))\boldsymbol{\gamma}_\beta(t),\end{aligned} \tag{8}$$

where

$$\zeta_\eta(\boldsymbol{x}) = \frac{1}{\eta^3}\zeta\left(\frac{\boldsymbol{x}}{\eta}\right) \tag{9}$$

is an approximation of Dirac mass at scale η. Several choices can be made for ζ, see, for instance, Refs. [10] and [12] for the proof of convergence of such regularized models. In the following, we will use the so-called low-order algebraic kernel

$$\zeta(\boldsymbol{x}) = \frac{3}{4\pi|\boldsymbol{x}|_1^5} \tag{10}$$

with the pseudonorm $|\boldsymbol{x}|_L = \sqrt{\|\boldsymbol{x}\|^2 + L^2}$. Using the low-order algebraic kernel, the regularized vorticity $\boldsymbol{\omega}_\eta$ and velocity $\boldsymbol{u}_\eta$ now reads

$$\boldsymbol{\omega}_\eta(\boldsymbol{x},t) = \sum_{\alpha=1}^N \boldsymbol{\gamma}_\alpha \frac{3\eta^2}{4\pi|\boldsymbol{x}|_\eta^5}, \tag{11}$$

$$\boldsymbol{u}_\eta(\boldsymbol{x},t) = -\frac{1}{4\pi}\sum_{\alpha=1}^N \frac{\boldsymbol{x}-\boldsymbol{x}_\alpha}{|\boldsymbol{x}-\boldsymbol{x}_\alpha|_\eta^3} \times \boldsymbol{\gamma}_\alpha. \tag{12}$$

With this choice for ζ, the shape of the velocity field given by (4) remains the same apart from the Euclidean norm $\|\cdot\|$ which changes to the pseudonorm $|\cdot|_\eta$.

Idea 3: Self-interactions. We assume that the vortons interact with each other following the transposed version of Euler equations. Using the regularization, the transposed scheme written in terms of $\boldsymbol{r}_{\alpha\beta} = \boldsymbol{x}_\alpha - \boldsymbol{x}_\beta$ and $\boldsymbol{\gamma}_\alpha$ is

$$\begin{aligned}\dot{\boldsymbol{x}}_\alpha &= -\frac{1}{4\pi}\sum_{\beta=1}^N \frac{\boldsymbol{r}_{\alpha\beta}}{|\boldsymbol{r}_{\alpha\beta}|_\eta^3} \times \boldsymbol{\gamma}_\beta,\\ \dot{\boldsymbol{\gamma}}_\alpha &= -\frac{1}{4\pi}\sum_{\beta=1}^N \left(\frac{\boldsymbol{\gamma}_\alpha \times \boldsymbol{\gamma}_\beta}{|\boldsymbol{r}_{\alpha\beta}|_\eta^3} - \frac{3\boldsymbol{r}_{\alpha\beta}}{|\boldsymbol{r}_{\alpha\beta}|_\eta^5}(\boldsymbol{r}_{\alpha\beta}\cdot(\boldsymbol{\gamma}_\alpha \times \boldsymbol{\gamma}_\beta))\right).\end{aligned} \tag{13}$$

The new parameter η corresponds to the size of vortices. Allowing this new, unconstrained variable to be time dependent makes it possible to balance the vortex stretching term, hence reaching a statistically stationary regime.

Idea 4: Dynamical regularization. We assume that the regularization length scale is dynamically adjusted and can either increase under the effect of viscous diffusion or decrease because of vortex stretching. The impact of such dynamics can be obtained by integrating the Navier-Stokes equations written for vorticity,

$$\frac{\mathrm{D}\boldsymbol{\omega}}{\mathrm{D}t} = (\boldsymbol{\omega}\cdot\nabla^{\mathrm{T}})\boldsymbol{u} + \nu\Delta\boldsymbol{\omega}, \tag{14}$$

over a ball centered on $\boldsymbol{x}_\alpha$ with a radius $\epsilon \ll \eta$ and allowing for a time-dependent η. Keeping only the dominant terms in the sums and considering $\Delta\psi_\eta(\boldsymbol{x}) \approx \delta(x)$, we end up with

$$\dot{\boldsymbol{x}}_\alpha = \boldsymbol{u}_\eta(\boldsymbol{x}_\alpha, t), \tag{15}$$

$$\dot{\boldsymbol{\gamma}}_\alpha = 3\left(\frac{\dot{\eta}}{\eta} - 5\frac{\nu}{\eta^2}\right)\boldsymbol{\gamma}_\alpha + [\boldsymbol{\nabla}\boldsymbol{u}_\eta(\boldsymbol{x}_\alpha, t)]^{\mathrm{T}}\boldsymbol{\gamma}_\alpha. \tag{16}$$

Viscosity therefore has a damping effect and introducing a time dependence on η is a way of introducing a new free parameter and therefore a supplemental constraint on the dynamics. The time evolution obtained for the vortex strength (16) is very similar to what was obtained in Ref. [13] in the inviscid case.

Idea 5: Rapid distorsion by a large-scale flow. We consider that the vortons are embedded within a large-scale flow $\boldsymbol{U}$, with velocity strain tensor $\boldsymbol{\nabla}\boldsymbol{U}$. Then, we take into account the action of the large-scale flow on the vortons through an additional advection by the large-scale velocity field and additional stretching by the large-scale strain-rate tensor. In final, the vortons are then advected by the field $\boldsymbol{u} = \boldsymbol{u}_\eta + \boldsymbol{U}$ and stretched by $[\boldsymbol{\nabla}\boldsymbol{u}]^{\mathrm{T}} = [\boldsymbol{\nabla}\boldsymbol{u}_\eta]^{\mathrm{T}} + [\boldsymbol{\nabla}\boldsymbol{U}]^{\mathrm{T}}$.

Idea 6: Feedback on the large-scale flow. We consider the feedback of the vortons on the large-scale flow via the subgrid stress tensor τ_ℓ, where ℓ is a yet unspecified filtering scale.

B. Application to shear flow

1. Equations

The subgrid model described above is very general. We now provide an application of the method to the transition to turbulence in shear flow. We consider the simplest possible shear flow, given by the velocity field:

$$\boldsymbol{U}(\boldsymbol{x}, t) = a(t)\begin{bmatrix}\sin(k_s z)\\ 0\\ 0\end{bmatrix}, \tag{17}$$

where $k_s = \frac{2\pi}{L_s}$ $\boldsymbol{U}(\boldsymbol{x}, t)$ is divergence-free and is compatible with periodic boundary conditions used in numerical simulations. For simplicity, we assume that the time dependence of the large-scale flow is fully encoded in its amplitude $a(t)$ while its spatial shape remains the same. We will provide a dynamics for the amplitude a which involves viscous dissipation, energy exchange with the small-scale vortons, and a smooth random forcing term, needed to reach a statistically steady state. We will take a forcing of the form $\boldsymbol{f}(\boldsymbol{x}, t) = (2/L^3)f(t)\sin(k_s z)\mathbf{e}_x$, where $f(t)$ is a smooth random Gaussian process of average 0 and standard deviation f_0.

We can then write the equation governing the dynamics of vorticity filtered at a scale ℓ. We do so by convoluting the curl of Navier-Stokes equations with a mollifier $G_\ell(\boldsymbol{x}) = 1/\ell^3 G(\boldsymbol{x}/\ell)$ to obtain

$$D_t\boldsymbol{\omega}_\ell = \mathrm{S}_\ell\boldsymbol{\omega}_\ell + \boldsymbol{\nabla}\times[\boldsymbol{\nabla}\cdot\tau_\ell] + \nu\Delta\boldsymbol{\omega}_\ell + \boldsymbol{\nabla}\times\boldsymbol{f}_\ell, \tag{18}$$

where S_ℓ is the filtered shear stress and $\tau_\ell = \boldsymbol{u}_\ell\otimes\boldsymbol{u}_\ell - (\boldsymbol{u}\otimes\boldsymbol{u})_\ell$ is the subgrid stress tensor. Exploiting the scale separation between the vorton scale η and the shear scale L_s, we can choose $\eta \ll \ell \ll L_s$, allowing for the approximations

$$\boldsymbol{f}_\ell \approx \boldsymbol{f},$$
$$\boldsymbol{U}_\ell \approx \boldsymbol{U},$$
$$\boldsymbol{\omega}_\ell \approx \boldsymbol{\nabla}\times\boldsymbol{U}.$$

Under the previous assumptions, the 3D filtered Navier-Stokes equations (18) satisfied by the large-scale flow reduce to a scalar equation for its amplitude $a(t)$. To obtain the time evolution of $a(t)$, we project Eq. (18) onto the large-scale vorticity $\boldsymbol{\omega}_\ell = a(t)k_s\cos(k_s z)\boldsymbol{e}_y$, integrating over a square box

of volume $|\mathrm{V}| = L^3$ with $L = nL_s$, $n \in \mathbb{N}^*$ and rescaling by the factor $k_s^{-1}(L^3/2)^{-1}$. This yields the following equation for $a(t)$:

$$\dot{a} = -\frac{a}{\tau_v^s} - \frac{3\pi^2\theta}{32L^3L_s\eta}\sum_{\alpha=1}^{N}\gamma_{\alpha,x}\gamma_{\alpha,z}\cos(k_s z_\alpha) + \frac{2}{L^3}f(t), \tag{19}$$

where $\theta \in [0, 1]$ is a coupling parameter depending on the choice of the filtering function used in (18) and $\tau_v^s = (\nu k_s^2)^{-1}$ is the large-scale viscous time. The derivation of the second term on the right-hand side, representing the contribution of the subgrid stress tensor, is given in Appendix B. Assuming the shape of $\boldsymbol{U}$ remains the same through time evolution is a very strong hypothesis. It is, however, possible to generalize the dynamics by considering the incompressible Galerkin truncated field:

$$\boldsymbol{U}(\boldsymbol{x}, t) = \sum_{|\boldsymbol{n}|<M} \boldsymbol{a_n}(t)e^{ik_s\boldsymbol{n}\cdot\boldsymbol{x}}.$$

The time evolution of the Fourier modes $\boldsymbol{a_n}(t)$ will be derived in the same fashion as we did for a. Tthe cutoff M must be chosen such that the large-scale separation hypothesis is still valid or, in other words, $Mk_S\eta \ll 1$. In this paper, we keep the toy model as simple as possible and therefore keep this idea for future work. We mention, in addition, that one could consider the large-scale field $\boldsymbol{U}$ to be the solution of a Large Eddy Simulation (LES). The embedding of vortex particles in LES flow has been studied in Ref. [14].

Taking into account the rapid distorsion of vortons by the large-scale shear flow, we then obtain the system of equations governing the vorton dynamics:

$$\dot{\boldsymbol{x}}_\alpha = \boldsymbol{u}(\boldsymbol{x}_\alpha, t) + \boldsymbol{U}(\boldsymbol{x}_\alpha, t), \tag{20}$$

$$\dot{\boldsymbol{\gamma}}_\alpha = 3\left(\frac{\dot{\eta}}{\eta} - 5\frac{\nu}{\eta^2}\right)\boldsymbol{\gamma}_\alpha + [\nabla\boldsymbol{u}(\boldsymbol{x}_\alpha, t)]^{\mathrm{T}}\boldsymbol{\gamma}_\alpha + [\nabla\boldsymbol{U}(\boldsymbol{x}_\alpha, t)]^{\mathrm{T}}\boldsymbol{\gamma}_\alpha. \tag{21}$$

To close this system, we have to provide the time evolution for η.

2. Closure for the regularization length

The closure of the system of equation is based on a kinetic energy budget between vortons and the large-scale flow. The (approximate) vorton kinetic energy is computed in Appendix A. It is given by

$$K_v = \frac{\Gamma}{64\eta}, \tag{22}$$

where Γ is defined in (7). On the other hand, the kinetic energy of the shear flow integrated over the box of volume $|\mathrm{V}| = L^3$ is

$$K_s = \frac{a^2L^3}{4}. \tag{23}$$

In the inviscid and nonforced case, kinetic energy should be exchanged between vortons and shear but conserved overall. We then consider two limiting situations: in the very viscous limit $\nu \gg 1$, the regularization length is just set by viscosity, so on dimensional ground $\dot{\eta} \sim \nu/\eta$, like the core-spreading method [4] (Sec. 5.6.2). In the inviscid limit $\nu \to 0$, the regularization length scale is evolving to keep $K = K_s + K_v$ constant. Patching the two behaviors, we get the following equation for η:

$$\dot{\eta} = 2\delta\frac{\nu}{\eta} - \frac{2\eta}{5\Gamma}\left[\langle\boldsymbol{\gamma}|\nabla\boldsymbol{u}^{\mathrm{T}}\boldsymbol{\gamma}\rangle + \left(1 - \frac{3\pi}{4}\theta\right)\langle\boldsymbol{\gamma}|\nabla\boldsymbol{U}^{\mathrm{T}}\boldsymbol{\gamma}\rangle\right], \tag{24}$$

where δ is a free parameter and we use the shorthand notation

$$\langle \boldsymbol{\gamma} | A \boldsymbol{\gamma} \rangle = \sum_{\alpha=1}^{N} \boldsymbol{\gamma}_\alpha^{\mathrm{T}} A(\boldsymbol{x}_\alpha, t) \boldsymbol{\gamma}_\alpha \tag{25}$$

for any tensor field $A(\boldsymbol{x}, t)$.

3. Choice of the parameters

There are two free parameters in the model, θ and δ.

(i) The parameter $\theta \in [0, 1]$ is a coupling parameter. We have no physical argument to select a particular value, so we use a choice that simplifies the equations, namely, we will take $\theta = 4/3\pi$ to cancel the contribution from the large-scale field to the dynamics of the regularization length (24). This choice simplifies the model and makes the interaction between the large-scale field and the vortons independent of the choice of the scale filter.

(ii) The parameter δ controls the viscous decay of the regularization length. In the case $\delta = 5/2$, viscous diffusion is entirely accounted for by the spreading of the vortex core, while the vortons intensities γ_α are not affected (21). In the other limiting case, $\delta = 0$, the vortex core size is not affected by viscosity, viscous dissipation thus only affects the vortons intensities. Thus, we should have $\delta \in [0, 5/2]$.

4. Control parameters

As we will see in the following sections, the statistics of the model are governed by the two physical input parameters: the viscosity ν and forcing amplitude f_0. These parameters can be used to build a dimensionless number usually referred to as the Grashof number:

$$\mathrm{Gr} = \frac{2 f_0}{\nu^2}. \tag{26}$$

Then, to study the hydrodynamics of the model, we can define a Reynolds number based on the fluctuations of the large-scale field,

$$\mathrm{Re} = \frac{\sigma_a L_s}{\nu}, \tag{27}$$

where $\sigma_a^2 = \mathbb{E} a^2$ is the variance of the shear flow amplitude, depending on f_0 and ν. This definition only makes sense if a reaches a statistically steady state. This will indeed be the case in both the laminar and turbulent states described later.

C. Diagnostics and global quantities

Diagnostics will be made using several global quantities based upon a and the fields $\boldsymbol{u}_\eta$ and $\boldsymbol{\omega}_\eta$. *A priori*, these global quantities depend on η and on the configuration $\{\boldsymbol{x}_\alpha, \boldsymbol{\gamma}_\alpha\}$. In practice, observables with a quadratic dependence on $\boldsymbol{u}_\eta$ and $\boldsymbol{\omega}_\eta$ will depend at first order on $\Gamma = \sum_\alpha \|\boldsymbol{\gamma}_\alpha\|^2$ and η. This was indeed the case for K_v given by Eq. (22) This is the case, for instance, for:

(i) The vorton dissipation rate that can be computed using Eqs. (20), (21), and (24) as

$$\dot{K}_v = (3 - \delta) \frac{5}{32} \frac{\Gamma}{\eta^3}. \tag{28}$$

(ii) The global energy dissipation $\dot{K}$, that can be computed using Eqs. (19) and (28) as

$$\dot{K} = f(t) a(t) - \nu \left[2\pi^2 a^2 \frac{L^3}{L_s^2} + (3 - \delta) \frac{5}{32} \frac{\Gamma}{\eta^3} \right]. \tag{29}$$

We see that since $\delta < 5/2$, the contribution of vortons in the total energy budget (29) is negative.

(iii) The vorton enstrophy:

$$\Omega \equiv \int \boldsymbol{\omega}_\eta^2(\boldsymbol{x}, t)^2 \, d^3x \approx \frac{45}{1024} \frac{\Gamma}{\eta^3}. \tag{30}$$

(iv) The vorton mean-squared velocity gradient:

$$S^2 \equiv \int (\nabla u_\eta(\boldsymbol{x}, t))^2 \, d^3x \approx \frac{15}{128} \frac{\Gamma}{\eta^3}. \tag{31}$$

Here, it is important to emphasize that since $\boldsymbol{\omega}_\eta$ is not divergence-free, the vorton enstrophy and their mean-squared velocity gradient do not coincide, unlike in solutions of the Navier-Stokes equations.

IV. RESULTS

A. Parameters

In this section, we present the results of simulations of the model described previously. We simulate $N = 3^3 = 27$ vortons in a periodic box of size $L = L_s = 1$. The vortons are initially placed on a regular cubic lattice with $3 \times 3 \times 3$ points spaced by $h = L/N^{1/3}$. The forcing is chosen as

$$f(t) = f_0 \left(\alpha_0 + \sqrt{2} \sum_{j=1}^{m} \left[\alpha_j \cos\left(2\pi j \frac{t}{T_f} \right) + \beta_j \sin\left(2\pi j \frac{t}{T_f} \right) \right] \right), \tag{32}$$

where T_f is the forcing period, $m = \lfloor T_f/\lambda \rfloor$, with $1/\lambda$ the maximum frequency of the forcing. The random part of the forcing comes from α_i, β_i, which are independent and identically distributed Gaussian variables of average 0 and standard deviation $1/(2m+1)$. In the end, the forcing term is smooth given the finite number of modes, T_f periodic, and of standard deviation f_0.

Regarding the parameters, we adopt $\theta = 4/3\pi$ and $\delta = 9/4$. This last value is chosen so the dissipation rate of the vortons (28) is indeed given by νS^2, with S^2 given by (31). Other parameters are taken as $\lambda = 1$, $T_f = 3000\lambda$. The intensities of the vortons are initialized taking their components as independent random variables distributed uniformly in $[-I, I]$ with $I = 10$. The simulation time is taken as T_f. We integrate the model using the standard Runge-Kutta method of order 5(4) implemented within the SciPy Python library.

B. Laminar and turbulent regimes

An interesting feature of this model is the existence of a transition between two regimes, highlighted by the ratio of mean energy dissipation at large scale $\langle \varepsilon_a \rangle = 2\pi^2 \nu L^3 / L_s^2 \langle a^2 \rangle$ to the mean injected power $\langle \mathrm{P_{inj}} \rangle = \langle a(t) f(t) \rangle$ as a function of the Reynolds number, which is shown in Fig. 1. At low Reynolds number ($\mathrm{Re} < \mathrm{Re}_c \approx 10^3$), this ratio is close to one, showing that all the dissipation is provided by the large-scale shear. This is confirmed by the time series shown in Fig. 2(e). In this regime, the regularization length grows continuously as the square root of time [Fig. 2(a)]. This means that the dynamics is mostly diffusive. In analogy with classical turbulence, we can identify this regime as laminar. In this laminar regime, the diffusive effects are dominating the whole dynamics allowing some approximations. The way we define the laminar regime is thus given by the set of equations (33) to (36) investigated in the following. At the critical Reynolds number $\mathrm{Re} = \mathrm{Re}_c$, there is a sudden drop in the ratio, followed by a new regime where the ratio is close to 0. This means that in this regime ($\mathrm{Re} > \mathrm{Re}_c$), energy is mostly dissipated by the vortons, as confirmed again in the time series shown in Fig. 2(f). In this regime, the regularization length scale reaches a statistically stationary value [Fig. 2(b)]. We call this regime the turbulent regime.

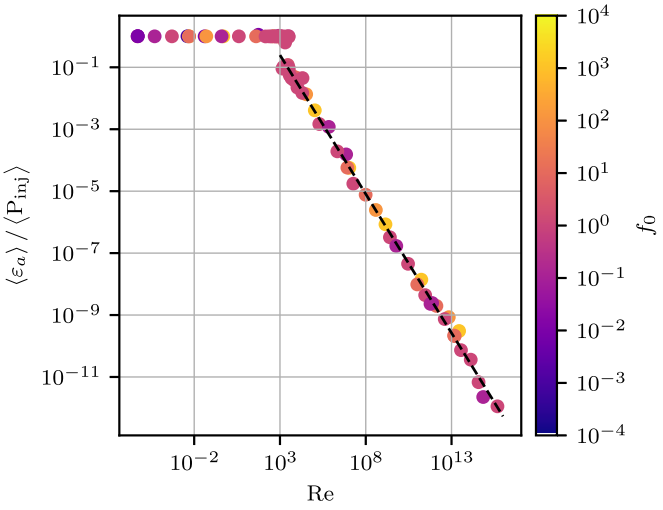

FIG. 1. Time-averaged dissipation rate for the large-scale flow normalized by the average injection rate as a function of the Reynolds number. The transition from a laminar state to a turbulent one occurs at $\mathrm{Re}_c \approx 10^3$ (or $\mathrm{Gr}_c \approx 2 \times 10^6$). For $\mathrm{Re} \leqslant \mathrm{Re}_c$, the injected power is dissipated by the large-scale flow while in the turbulent regime, energy is dissipated at a smaller vorton scale. The ratio of the large-scale dissipation rate to the injected power decreases in the turbulent regime following a power law with fitted exponent $\alpha = -0.90$.

The laminar to turbulent transition is also observed in the behavior of other global variables, such as the mean regularization length as a function of Reynolds number; see Fig. 3. In the laminar regime, its value is mainly constrained by the finite simulation time T_f as it grows continuously, while in the turbulent regime it scales as a power law $\langle \eta \rangle \sim \mathrm{Re}^{\alpha}$ with $\alpha \approx -0.44$. We also observe the transition in the relation between Reynolds number scaling and the Grashof number shown in Fig. 4. At low value of Reynolds and Grashof, the scaling is linear, while at higher values of the Grashof number the scaling is different with $\mathrm{Re} \sim \mathrm{Gr}^{\alpha}$ with $\alpha \approx 0.52$. In steady state turbulence, it is observed [15] that the variance of the velocity field becomes independent of viscosity in the limit of vanishing viscosity. In our model, this would be verified if $\alpha = 1/2$, as if $\mathrm{Re} \sim \mathrm{Gr}^{\alpha}$ we should have $\sigma_a \sim f_0^{\alpha} \nu^{1-2\alpha}$. As shown in Fig. 4, the scaling exponent fitted on our simulations results is close to $1/2$ but slightly larger (the 95% confidence interval does not include $1/2$).

C. Dynamics in the laminar regime

We can further explore the dynamics of the model in the laminar regime by simplifying the equations, neglecting the vorton-vorton interactions and the retroaction of the vortons on the large-scale flow. The system then reduces to

$$\dot{a} = -\frac{a}{\tau_\nu^s} + \frac{2}{L^3} f(t), \tag{33}$$

$$\dot{\eta} = 2\delta \frac{\nu}{\eta}, \tag{34}$$

$$\dot{\boldsymbol{x}}_\alpha = \boldsymbol{U}(\boldsymbol{x}_\alpha, t), \tag{35}$$

$$\dot{\boldsymbol{\gamma}}_\alpha = 3(2\delta - 5)\frac{\nu}{\eta^2}\boldsymbol{\gamma}_\alpha + \boldsymbol{\nabla U}^{\mathrm{T}}(\boldsymbol{x}_\alpha, t)\boldsymbol{\gamma}_\alpha. \tag{36}$$

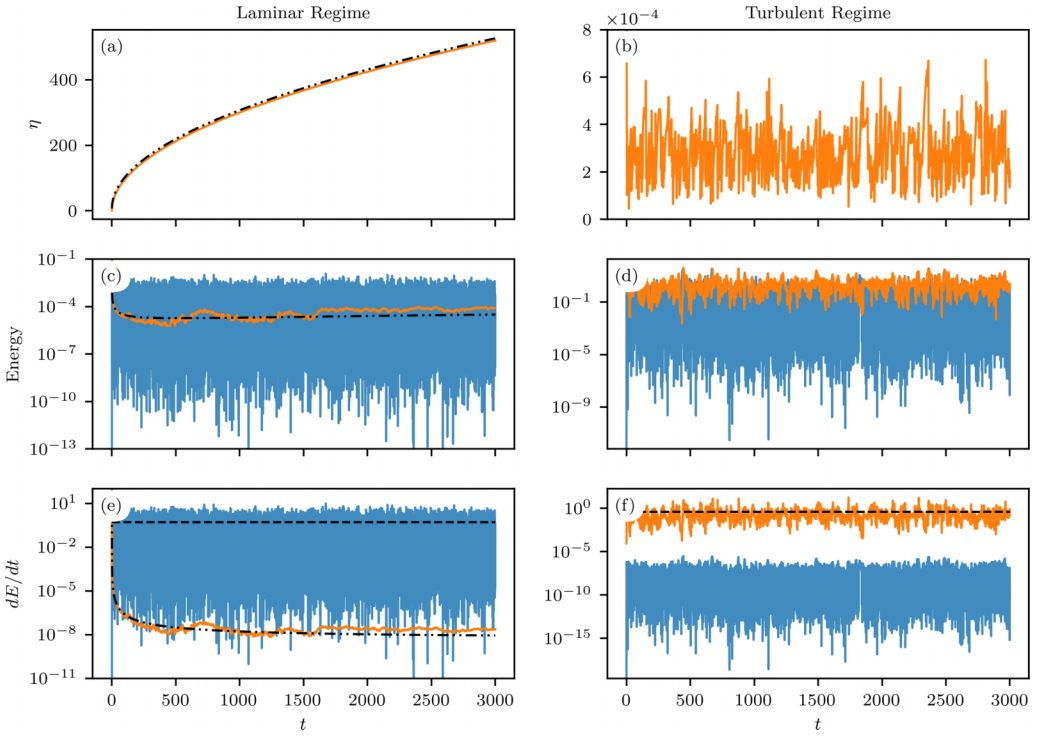

FIG. 2. Time series of regularization length (a), (b); kinetic energy (c), (d); and viscous dissipation and injected power (e), (f) in the laminar [left column: (a), (c), (e)] and turbulent [right column: (b), (d), (f)] regimes. The two regimes are both illustrated by the results of a single simulation with control parameters $\nu = 10$ (respectively, $\nu = 10^{-9}$) and $f_0 = 10$ (respectively, $f_0 = 1$) for the laminar (turbulent) regime. The first row (a), (b) shows the time series of the regularization length. In the laminar regime (a), its dynamics matches the prediction $f_1(t) = \eta_0 \psi(t)$ (represented by the dash-dotted black line, slightly offset for readability) while it reaches a stationary mean value in the turbulent regime (b). The second row (c), (d) shows the time series of both the large-scale kinetic energy (blue line) and of the vorton kinetic energy (orange line). In the laminar regime (c), the kinetic energy of the vortons follows well the expected dynamics at large timescales represented by the dash-dotted black line $[f_2(t) = (1/64\eta_0)(I^2/4)\psi(t)^{\frac{(5\delta-15)}{\delta}}(1 + t(t + T_f)/((2m + 1)\tau_\Gamma^2))]$. The last row (e), (f) depicts the energy budget with the dissipation from the large-scale flow (blue line), that from the vortons (orange line) and the time-averaged injected power (dashed horizontal black line). In the laminar regime, energy injection is mostly balanced by dissipation at large scale while in the turbulent regime, energy injection is balanced by dissipation at small scales, i.e., by the vortons. Additionally, the dissipation from vortons matches well with the expected dynamics at large timescales represented by the dash-dotted black line $[(f_3(t) = (15/128\eta_0^3)(I^2/4)\psi(t)^{\frac{(3\delta-15)}{\delta}}[1 + t(t + T_f)/((2m + 1)\tau_\Gamma^2))]]$.)

To simplify future computation, we will also consider that the large scale flow is overdamped, yielding

$$a(t) = a_{\text{rms}}\left(\frac{f(t)}{f_0}\right),$$

with $a_{\text{rms}} = (1/4\pi^2)(L_s^2/L^3)(2f_0/\nu)$ the standard deviation of a. Under these assumptions, the Reynolds number should thus behave in the laminar regime as

$$\text{Re} = \left(\frac{L_s}{L}\right)^3 \frac{\text{Gr}}{4\pi^2}. \tag{37}$$

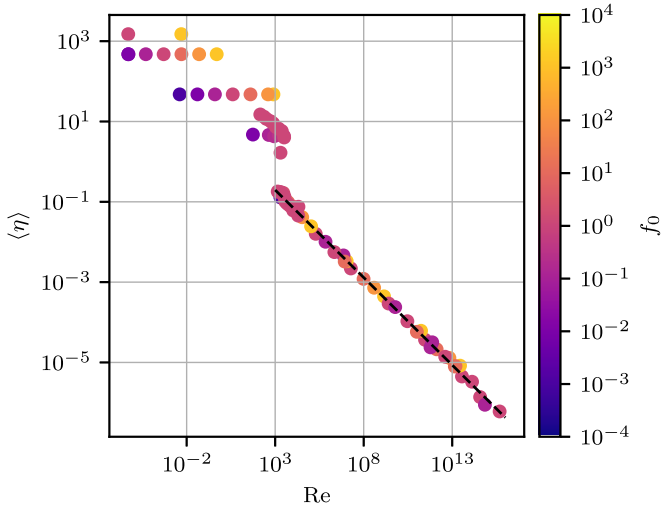

FIG. 3. Mean regularization length as a function of the Reynolds number. Each dot corresponds to a single simulation, with given values of viscosity ν and forcing amplitude f_0 (f_0 being represented by the dot color). Two regimes can be identified, separated by a critical Reynold number $\mathrm{Re}_c \sim 1000$, where the regularization length either grows as the square root of time in the laminar regime (low Reynolds numbers) or reaches a stationary mean value in the turbulent regime (high Reynolds numbers). The black dashed line is a fit of a power law $< \eta > \sim \mathrm{Re}^{\alpha}$ in the turbulent regime, with fitted exponent $\alpha = -0.44$. For $\mathrm{Re} \leqslant \mathrm{Re}_c$, η behaves as $\sqrt{\eta_0^2 + 4(1-\delta)\nu t}$. The finite values observed here are due to the finite time of the simulation and are indeed independent of the forcing amplitude f_0.

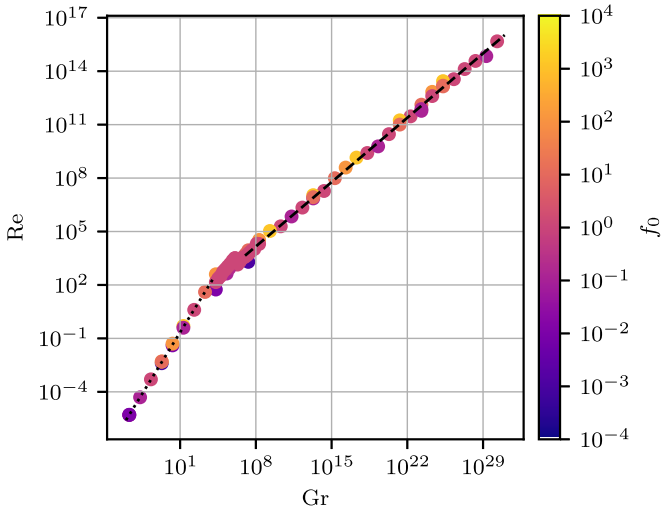

FIG. 4. Reynolds number $\mathrm{Re} = \sigma_a L_s/\nu$ as a function of Grashof number $\mathrm{Gr} = 2f_0/\nu^2$. Each dot corresponds to a single simulation, with given values of viscosity ν and forcing amplitude f_0 (f_0 being represented by the dot color). The dotted and dashed lines are power law fits of the two regimes (laminar and turbulent). The fitted exponents are $\alpha = 0.99$ for the laminar regime and $\alpha = 0.52$ for the turbulent regime. The scaling for the laminar regime match the prediction (37).

The scaling derived in Eq. (37) is indeed consistent with the numerical results shown in Fig. 4, with the Reynolds number scaling as the Grashof number for $\mathrm{Gr} < \mathrm{Gr_c} \approx 10^5$.

Time dependence of various physical quantities such as the regularization scale, and the forcing terms are computed in Appendix C. Using these estimates, we find that the vorton kinetic energy $K_v = \Gamma/(64\eta)$, energy dissipation $\dot{K}_v = (3-\delta)\frac{5}{32}\frac{\Gamma}{\eta^3}$, or enstrophy $\Omega_v = 45\Gamma/(2048\eta^3)$, are thus, respectively, behaving as $t^{\frac{9\delta-15}{2\delta}}$, $t^{\frac{7\delta-15}{2\delta}}$, and $t^{\frac{7\delta-15}{2\delta}}$ when $t \to \infty$. Energy would thus decrease with time in the laminar regime if $\delta < 15/9$ while energy dissipation or enstrophy would decrease if $\delta < 15/7$. With our choice of $\delta = 9/4$, both K_v and $\dot{K}_v$ should increase indefinitely at large times, which is unrealistic. However, one should keep in mind that the regularization length η increases indefinitely and eventually becomes larger than the size of the periodic box L, which is not physical. As η increases, the vorton field is not concentrated at small scales anymore (the cutoff wave number in the energy spectrum is $1/\eta$). Consequently, the increase of the vortons kinetic energy is likely due to the progressive accumulation of energy at larger and larger spatial scales. We represent the expected dynamics at large timescales in Figs. 2(c) and 2(d) for the energy of the vortons and their energy dissipation. These laws are indeed well verified.

D. Dissipation rate

One of the main hypothesis of Kolmogorov turbulence phenomenology [15] is that the energy dissipation rate becomes independent of viscosity in the limit of vanishing viscosity, and that it should scale with the cube of the standard deviation of the velocity field. This is indeed observed in numerical simulations [16] or experiments like the von Karman flow [17]. In the case of shear flows, this scaling depends on the boundary conditions via the state of the surface [18]: For rough surfaces, this scaling is indeed observed, while for smooth surfaces, present data only evidence a slow decay with with decreasing viscosity, possibly corresponding to logarithmic corrections.

In the present case, the energy dissipation comes from two sources $\varepsilon = \varepsilon_a + \varepsilon_v$, where ε_a denotes the dissipation coming from the large scale shear, while ε_v corresponds to the dissipation due to the vortons. Normalizing by σ_a^3/L_s, we then get

$$\frac{\langle \epsilon \rangle}{\sigma_a^3/L_s} = \frac{2\pi^2 L^3}{\mathrm{Re}} + \frac{1}{\mathrm{Re}}\left(\frac{L_s}{\sigma_a}\right)^2 (3-\delta)\frac{5}{32}\left\langle \frac{\Gamma}{\eta^3}\right\rangle. \tag{38}$$

The first term scales as the inverse of the Reynolds number and corresponds to the large-scale dissipation. The second term represents the contribution of the vortons. These two contributions are plotted in Fig. 2 both in the laminar and the turbulent regime. Before the transition, the dissipation due to the large scale flow indeed dominates, while in the turbulent regime the vorton dissipation dominates. These two regimes pilot the behavior of the total energy dissipation as a function of the Reynolds number, shown in Fig. 5.

Before the transition, the normalized dissipation rate indeed behaves as the inverse of the Reynolds number, while in the turbulent regime, we observe a slower power law decay with a higher dispersion, which may be due to slower convergence, see below. This second regime can be fitted with a power law with a small exponent $\alpha = -0.10$ that could be the signature of logarithmic corrections.

The scatter observed in the turbulent regime may be traced to the high intermittency of the energy dissipation, in analogy with what is observed in homogeneous isotropic turbulence [15]. In our case, again in agreement with homogeneous isotropic turbulence [17], the statistics of energy dissipation can be well approximated by a log-normal random distribution, see Fig. 6.

V. DISCUSSION

We have introduced a toy model of shear flows, exploiting the spatial intermittency and the scale separation between the large-scale flow and the small-scale structures. The model is very sparse, as only the most intense structures are considered, which are modeled via vortons, representing

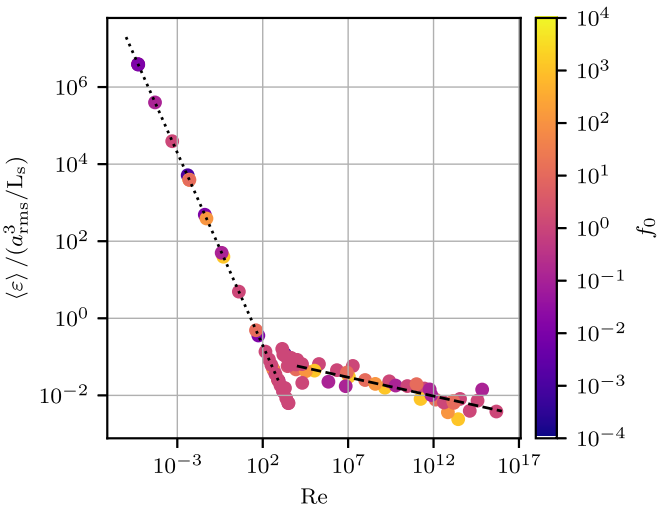

FIG. 5. Rescaled total dissipation rate as a function of the Reynolds number. Similarly to turbulent flow, the dissipation rate scales as the cube of the velocity field variance. In the laminar regime, the rescaled dissipation scales as Re^{-1} (the fitted coefficient is $\alpha = -1.00$), while in the turbulent regime, we get a smaller exponent ($\alpha = -0.10$), and the data points being quite scattered.

dynamically regularized quasisingularities subject to rapid distorsion by the large-scale shear, and which retroact on this large-scale flow via the subgrid stress. The model displays an interesting transition between two regimes: (i) a laminar regime, in which all the dissipation is accounted for

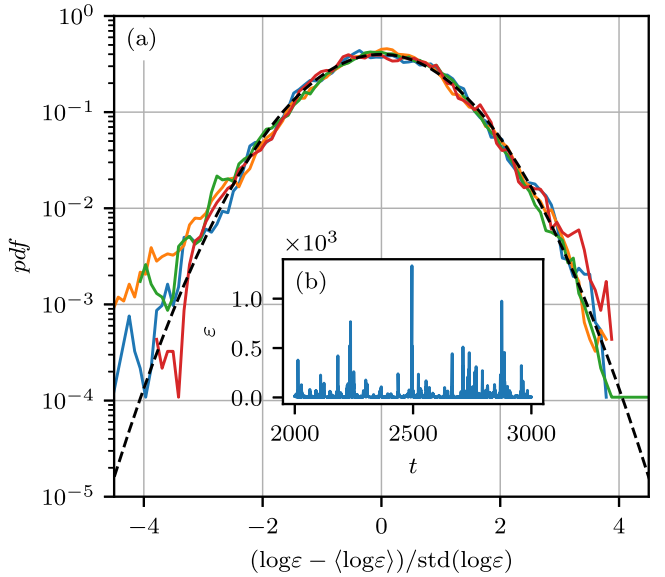

FIG. 6. (a) Standardized probability density function (PDF) of the dissipation rate logarithm for different Reynolds numbers in the turbulent state. The dashed black line correspond to to the normal distribution. The blue, orange, green, and red lines, respectively, correspond to $\mathrm{Re} = 8.84 \times 10^3$; 9.84×10^7; 1.32×10^{12}; 1.67×10^{14}. (b) Time series of the dissipation rate (for $\mathrm{Re} = 1.32 \times 10^{12}$), showing its highly intermittent dynamics characterized by strong bursts of dissipation separated by relatively quiescent time intervals.

by the large-scale flow, and the vorton dynamics is essentially diffusive; and (ii) a turbulent regime, in which most of the dissipation is produced by the vortons. These two regimes correspond to different scalings of the dissipation and the Grashof number as a function of Reynolds, with power laws that resembles the laws observed in classical turbulence.

This shows that, despite its simplicity, our toy model may be of interest to understand or reproduce some of the observed properties of shear flows. As it stands, our model cannot be used directly for subgrid modeling of shear flows, as it includes several arbitrary parameters that would need calibration against a Direct Numerical Simulation (DNS) of Navier-Stokes equations, at least in the idealized case of fully developed 3D turbulence with strong imposed shear (e.g., flow over a flat plate, Couette flow). Using physical arguments, we tried to decrease as much as possible the number of free parameters in our model, but actually two of them remain, namely, the coupling parameter θ and the parameter controlling viscous dissipation δ. In addition, there might exist an optimum for the number of vortons we need to use. We have found that increasing the density of vortons by a factor 4.6 does not change the results, but there may exist an optimal value of the density to get better agreement with DNS. In addition, our representation of the feedback between vortons and the mean shear is limited to the case where the large scale flow is overdamped and does not change shape due to the interaction. A perhaps more realistic computation could include an additional mode describing the large scale shear, at the expense of simplicity. Finally, we did not systematically vary the parameters of the forcing (its shape and maximum frequency) to check its influence.

In the spirit of understanding at least qualitatively what the influence of various additional mechanisms are on shear flow dynamics, one could, however, try to modify the toy model to study specific effects. For example, in this preliminary validation, we neglected the feedback on the profile shape of the large-scale flow by introducing an *ad hoc* forcing. This situation is perhaps more realistic in geophysical flows, where external forces such as solar irradiance and the Coriolis force determine a velocity and temperature gradient that do not deviate too much from quasigeostrophy and adiabatic profile, at least in the midlatitudes. In the case of shear flows forced by boundary conditions (Couette flow) or via a constant pressure gradient (Poiseuille), we know that this condition is not realistic, as the turbulent fluctuations are known to flatten the global shear in the middle of the domain. Even if we consider the layer just above the boundary layer, it is well-known that the velocity profile switches from linear to logarithmic. As discussed in Refs. [1–3], this effect can be explained via rapid distorsion theory, which predicts that the $x - y$ component of the subgrid stress tensor scales inversely with the local large-scale shear, leading to the log-law of the wall after integration. Due to our approximation, we cannot capture this effect here, but it would be interesting to generalize our model to take into account the local shear. Note that all the computations made in Refs. [1–3] use localized Gaussian wave packets of vorticity that are very close in spirit to our quasisingularities. The main difference comes from our dynamical regularization, which may introduce unique effects. Another interesting generalization would be toward geophysical flows, and especially localized extreme events such as convective storms. Indeed, individual convective cells are relatively sparse, and move within the synoptic (large-scale) wind and temperature fields, while interacting with nearest neighbors. If conditions are favorable, they can further organize into clusters known as mesoscale convective systems [19], which can produce a significant hazard. An example of such severe storms are derechos, which are long-lived mesoscale convective storms producing widespread severe surface wind gusts [20]. To deal with convective systems, one needs to add the coupling between temperature and velocity, as well as moisture effect. Work is currently in progress to generalize our model to describe such types of coherent structures.

ACKNOWLEDGMENTS

This work received funding from the Ecole Normale Supérieure de Lyon, from ANR TILT Grant Agreement No. ANR-20-CE30-0035, from ANR BANG Grant Agreement No.

ANR-22-CE30-0025, from the CNRS Program Recherche Risques ALEAS, and from the CEA program Focus Numérique Frugal.

DATA AVAILABILITY

The data that support the findings of this article are not publicly available. The data are available from the authors upon reasonable request.

APPENDIX A: KINETIC ENERGY

To derive the kinetic energy of the vorton field, we can first derive the expression for the energy spectrum of the vorton field:

$$E(\rho,t)=\frac{1}{2}\int_{\mathbb{S}^2(0,\rho)}\|\widehat{\boldsymbol{u}}(\boldsymbol{k},t)\|^2\mathrm{d}\boldsymbol{k}. \tag{A1}$$

To do so, let us first write the Fourier transform of the vorton velocity field:

$$\widehat{u}^m_\eta(\boldsymbol{k})=-\varepsilon_{m,n,p}\frac{i}{4\pi}\frac{k^n\eta K_1(\eta|\boldsymbol{k}|)}{|\boldsymbol{k}|}\sum_{\alpha=1}^{N}e^{-i\boldsymbol{k}\cdot\boldsymbol{x}_\alpha}\gamma^p_\alpha, \tag{A2}$$

where K_1 is the second type modified Bessel function of order one and $\varepsilon_{m,n,p}$ is the Levi-Civita symbol. We then obtain the one-dimensional energy spectrum (A1):

$$E(\rho,t)=\frac{[\eta\rho K_1(\eta\rho)]^2}{2\pi}\left[\frac{2}{3}\Gamma+\sum_{\substack{\alpha,\beta\\ \alpha\neq\beta}}(\boldsymbol{\gamma}_\alpha\cdot\boldsymbol{\gamma}_\beta)\phi_1(2\pi\rho\|\boldsymbol{r}_{\alpha\beta}\|)+\frac{\boldsymbol{\gamma}_\alpha\cdot\boldsymbol{r}_{\alpha\beta}}{\|\boldsymbol{r}_{\alpha\beta}\|}\frac{\boldsymbol{\gamma}_\beta\cdot\boldsymbol{r}_{\alpha\beta}}{\|\boldsymbol{r}_{\alpha\beta}\|}\phi_2(2\pi\rho\|\boldsymbol{r}_{\alpha\beta}\|)\right] \tag{A3}$$

with $\Gamma=\sum_\alpha\|\boldsymbol{\gamma}_\alpha\|^2$ and

$$\begin{aligned}\phi_1(z)&=z^{-3}((z^2-1)\sin z+z\cos z)\\ \phi_2(z)&=z^{-3}((3-z^2)\sin z-3z\cos z).\end{aligned} \tag{A4}$$

The total kinetic energy energy of the vorton-induced field is given by the integral of Eq. (A3) along ρ. This integral cannot be computed analytically for a finite η except for the first term, which is the dominant one for the total kinetic energy in the small η limit since it is independent of ρ. The dominant contribution to kinetic energy thus reads

$$K_v=\frac{\Gamma}{64\eta}. \tag{A5}$$

APPENDIX B: DERIVATION OF THE SUBGRID STRESS TENSOR TERM IN THE LARGE-SCALE FLOW AMPLITUDE EQUATION

As explained in Sec. III B 1, we obtain the time evolution of the large-scale shear amplitude by computing

$$k_s^{-1}(L^3/2)^{-1}\int_{\mathrm{V}}(18)\cdot\mathbf{e}_y\cos(k_sz)\,\mathrm{d}\boldsymbol{x}. \tag{B1}$$

To compute specifically the contribution of the subgrid stress tensor, we begin by noting that

$$\int(\cos(k_sz)\mathbf{e}_y)\cdot(\boldsymbol{\nabla}\times[\boldsymbol{\nabla}\cdot\tau_\ell])\mathrm{d}x=-k_s^2\mathrm{Re}\big(\widehat{\tau}_\ell^{z,x}(k_s\mathbf{e}_z)\big), \tag{B2}$$

where we used two integration by parts, $\widehat{\tau_\ell}$ being the Fourier transform of the subgrid stress tensor whose components are written as exponents. As the only nonzero component of the large scale velocity field is U^x, we get

$$\widehat{\tau_\ell^{z,x}} \approx \widehat{U_\ell^x u_{\eta,\ell}^z} - \widehat{\left(U^x u_\eta^z\right)_\ell} + \widehat{u_{\eta,\ell}^x u_{\eta,\ell}^z} - \widehat{\left(u_\eta^x u_\eta^z\right)_\ell}. \tag{B3}$$

With Eq. (A2), we have

$$\widehat{U^x u_\eta^z}(\boldsymbol{k}) = \frac{a}{2i}\left[\widehat{u_\eta^z}(\boldsymbol{k} - k_s\mathbf{e}_z) - \widehat{u_\eta^z}(\boldsymbol{k} + k_s\mathbf{e}_z)\right], \tag{B4}$$

which vanishes when evaluated at $\boldsymbol{k} \propto \mathbf{e}_z$ because $\varepsilon_{z,z,p} = 0$ in (A2). Assuming further that $(U u_\eta)_\ell \approx U_\ell u_{\eta,\ell}$, we are left with the computation of

$$\widehat{\tau_\ell^{z,x}}(k_s\mathbf{e}_z) = \widehat{u_{\eta,\ell}^x u_{\eta,\ell}^z}(k_s\mathbf{e}_z) - \widehat{\left(u_\eta^x u_\eta^z\right)_\ell}(k_s\mathbf{e}_z). \tag{B5}$$

By definition of the filtered velocity field, writing $\boldsymbol{p} = k_s\mathbf{e}_z$, one has

$$\widehat{\tau_\ell^{z,x}}(\boldsymbol{p}) = \int g_\ell(\boldsymbol{q}, \boldsymbol{p})\widehat{u_\eta^x}(\boldsymbol{q})\widehat{u_\eta^z}(\boldsymbol{p} - \boldsymbol{q})\mathrm{d}\boldsymbol{q}, \tag{B6}$$

where $g_\ell(\boldsymbol{q}, \boldsymbol{p}) = [\widehat{G}(\ell\boldsymbol{q})\widehat{G}(\ell(\boldsymbol{p} - \boldsymbol{q})) - \widehat{G}(\ell\boldsymbol{p})]$ and G_ℓ is the filtering function. Injecting the Fourier transform of the velocity field and rescaling the integration variable by η, one obtains

$$\begin{aligned}\widehat{\tau_\ell^{z,x}}(\boldsymbol{p}) = \frac{\varepsilon_{1,m,n}\varepsilon_{3,\alpha,\beta}}{(4\pi)^2\eta}\sum_{j_1,j_2} e^{-i\boldsymbol{p}\cdot\boldsymbol{x}_{i_2}}\gamma_{j_1,n}\gamma_{j_2,\beta}\int g_\ell\left(\frac{\boldsymbol{q}}{\eta}, \boldsymbol{p}\right)\frac{q_m q_\alpha}{|\boldsymbol{q}||\eta\boldsymbol{p} - \boldsymbol{q}|}K_1(|\boldsymbol{q}|)K_1(|\eta\boldsymbol{p} - \boldsymbol{q}|) \\ \times e^{-i\frac{\boldsymbol{q}\cdot\boldsymbol{r}_{j_1 j_2}}{\eta}}\mathrm{d}\boldsymbol{q},\end{aligned} \tag{B7}$$

where we have used $\varepsilon_{3,\alpha,\beta}(\eta p_\alpha - q_\alpha) = -\varepsilon_{3,\alpha,\beta}q^\alpha$ because $\boldsymbol{p} \propto \mathbf{e}_z$. Then, we choose to mollify at a scale $\ell = \eta$ such that $\ell \ll L_s$ and we keep only the leading order term in ℓ/L_s. Moreover, considering that η is small compared to the average distance between two vortons, we keep only the resonant term $j_1 = j_2 = j$ in the sum. This yields

$$\widehat{\tau_\ell^{z,x}}(\boldsymbol{p}) = \frac{\varepsilon_{1,m,n}\varepsilon_{3,\alpha,\beta}}{(4\pi)^2\eta}\sum_j e^{-i\boldsymbol{p}\cdot\boldsymbol{x}_j}\gamma_{j,n}\gamma_{j,\beta}\int [\widehat{G}(\boldsymbol{q})^2 - 1]\frac{q_m q_\alpha}{|\boldsymbol{q}|^2}K_1(|\boldsymbol{q}|)^2\mathrm{d}\boldsymbol{q}. \tag{B8}$$

Then, as G is a real radial function, its Fourier transform is also isotropic, so we end up with

$$\widehat{\tau_\ell^{z,x}}(\boldsymbol{p}) = \frac{1}{4\pi\eta}\sum_j e^{-i\boldsymbol{p}\cdot\boldsymbol{x}_j}\gamma_{j,z}\gamma_{j,x}\int_0^\infty [1 - \widehat{G}(r)^2]r^2K_1(r)^2\mathrm{d}r. \tag{B9}$$

The value of the remaining integral depends on the choice of the mollifier and is between 0 and $3\pi^2/32$. We therefore introduce a parameter $\theta \in [0, 1]$ which will play the role of a coupling parameter between small scales and large scales such that the integral is equal to $(3\pi^2/32)\theta$. Therefore,

$$\Re\widehat{\tau_\ell^{z,x}}(k_s\mathbf{e}_3) = \frac{3\pi\theta}{128\eta}\sum_{\alpha=1}^N \gamma_{\alpha,z}\gamma_{\alpha,x}\cos(k_s z_\alpha), \tag{B10}$$

which yields the second term on the right-hand side of the amplitude equation (19) by substituting (B10) in (B2) and dividing by $k_s(L^3/2)$.

APPENDIX C: EXPECTED DYNAMICS IN THE LAMINAR REGIME

We can compute analytically the expected dynamics of several variables related to the vortons in the laminar regime. Vortons are advected by the shear flow only (35) and, in particular,

$$z_\alpha(t) = z_\alpha(0). \tag{C1}$$

Writing $\psi(t) = \sqrt{1 + 4\nu\delta t/\eta_0^2}$, Eq. (34) solves as

$$\eta(t) = \eta_0 \psi(t), \tag{C2}$$

and for $i = 1, 2$,

$$\gamma_{\alpha,i}(t) = \gamma_{\alpha,i}(0)\psi(t)^{\frac{3(2\delta-5)}{2\delta}}, \tag{C3}$$

while

$$\gamma_{\alpha,z}(t) = \psi(t)^{\frac{3(2\delta-5)}{2\delta}}\left(\gamma_{\alpha,z}(0) + \gamma_{\alpha,x}(0)\frac{2\pi}{L_s}\int_0^t a(s)\cos\left(\frac{2\pi}{L_s}z_\alpha(s)\right)\mathrm{d}s\right). \tag{C4}$$

Recalling that $z_\alpha(t) = z_\alpha(0)$ and taking random initial intensities following a uniform law given by $\gamma_{\alpha,i}(0) \hookrightarrow \mathcal{U}(-I/(2\sqrt{N}), I/(2\sqrt{N}))$, we end up with

$$\mathbb{E}\Gamma(t) = \frac{I^2}{4}\psi(t)^{\frac{3(2\delta-5)}{\delta}}\left[1 + \frac{2}{2m+1}\frac{t^2}{\tau_\Gamma^2}\sum_{j=0}^{m}\mathrm{sinc}^2\left(\frac{j\pi t}{T_f}\right)\right], \tag{C5}$$

where $\mathrm{sinc}(x) = \sin x/x$ and $\tau_\Gamma = \sqrt{12}\pi L^3\nu/(L_s f_0)$ and we also assumed that $N \geqslant 3^3$. At large time, the sum in Eq. (C5) behaves approximately (graphically) as $1/2(1 + T_f/t)$, while $\psi(t) \sim \sqrt{t}$. We then get

$$\begin{aligned}
\mathbb{E}\Gamma(t) &\underset{t\to\infty}{\propto} t^{\frac{10\delta-15}{2\delta}},\\
K_v(t) \sim \mathbb{E}\Gamma(t)/\psi &\underset{t\to\infty}{\propto} t^{\frac{9\delta-15}{2\delta}},\\
\dot{K}_v \sim \Omega(t) \sim \mathbb{E}\Gamma(t)/\psi^3 &\underset{t\to\infty}{\propto} t^{\frac{7\delta-15}{2\delta}}.
\end{aligned} \tag{C6}$$

[1] S. Nazarenko, Exact solutions for near-wall turbulence theory, Phys. Lett. A **264**, 444 (2000).

[2] S. Nazarenko, N. K. R. Kevlahan, and B. Dubrulle, Nonlinear RDT theory of near-wall turbulence, Physica D **139**, 158 (2000).

[3] B. Dubrulle, J. P. Laval, S. Nazarenko, and N. K.-R. Kevlahan, A dynamic subfilter-scale model for plane parallel flows, Phys. Fluids **13**, 2045 (2001).

[4] G.-H. Cottet and P. D. Koumoutsakos, *Vortex Methods: Theory and Practice* (Cambridge University Press, Cambridge, 2000).

[5] C. Mimeau and I. Mortazavi, A review of vortex methods and their applications: From creation to recent advances, Fluids **6**, 68 (2021).

[6] L. Onsager, Statistical hydrodynamics, Nuovo Cim. **6**, 279 (1949).

[7] E. A. Novikov, Generalized dynamics of three-dimensional vortex singularities (vortons), Zh. Eksp. Teor. Fiz. **84**, 975 (1983).

[8] D. Mumford and P. W. Michor, On Euler's equation and 'EPDiff,' J. Geom. Mech. **5**, 319 (2013).

[9] P. G. Saffman and D. I. Meiron, Difficulties with three-dimensional weak solutions for inviscid incompressible flow, Phys. Fluids **29**, 2373 (1986).

[10] G. Winckelmans and A. Leonard, Contributions to vortex particle methods for the computation of three-dimensional incompressible unsteady flows, J. Comput. Phys. **109**, 247 (1993).

[11] G. Winckelmans and A. Leonard, Weak solutions of the three-dimensional vorticity equation with vortex singularities, Phys. Fluids **31**, 1838 (1988).
[12] J.-P. Choquin, G.-H. Cottet, and R. Dautray, On the analisys of a class of three dimensional vortex method, C. R. Acad. Sci., Ser. I **306**, 739 (1988).
[13] E. J. Alvarez and A. Ning, Stable vortex particle method formulation for meshless large-eddy simulation, AIAA J. **62**, 637 (2024).
[14] N. Kornev and S. Samarbakhsh, Large eddy simulation with direct resolution of subgrid motion using a grid free vortex particle method, Int. J. Heat Fluid Flow **75**, 86 (2019).
[15] U. Frisch, *Turbulence: The Legacy of A.N. Kolmogorov* (Cambridge University Press, 1995).
[16] K. R. Sreenivasan, On the scaling of the turbulence energy dissipation rate, Phys. Fluids **27**, 1048 (1984).
[17] B. Dubrulle, Beyond Kolmogorov cascades, J. Fluid Mech. **867**, P1 (2019).
[18] G. Eyink, Onsager's 'ideal turbulence' theory, J. Fluid Mech. **988**, P1 (2024).
[19] R. A. Houze, 100 years of research on mesoscale convective systems, Meteorol. Monogr. **59**, 17.1 (2018).
[20] L. Fery and D. Faranda, Analysing 23 years of warm-season derechos in France: A climatology and investigation of synoptic and environmental changes, Weather Clim. Dynam. **5**, 439 (2024).